Ocean Engineering 220 (2021) 108437

Contents lists available at ScienceDirect

Ocean Engineering

journal homepage: www.elsevier.com/locate/oceaneng

Site-specific soil reaction model for monopiles in soft clay based on laboratory element stress-strain curves

Yongqing Lai [b], Lizhong Wang [b], Youhu Zhang [a,*], Yi Hong [b]

[a] Norwegian Geotechnical Institute, Sognsveien 72, 0855, OSLO, Norway
[b] Key Laboratory of Offshore Geotechnics and Material of Zhejiang Province, College of Civil Engineering and Architecture, Zhejiang University, China

ARTICLE INFO

Keywords:
Monopile
Soft clay
p-y curve
Base shear
Base moment
Stress-strain
Finite element analysis
Centrifuge modelling

ABSTRACT

Large-diameter monopiles are the predominant foundation solution for supporting offshore wind turbines. They are conventionally designed using soil reaction curves developed for long slender piles used for supporting offshore oil and gas platforms (e.g., the API *p-y* model). However, due to the difference in the length/diameter ratio and the resulting soil mechanisms, the use of *p-y* curves alone can lead to significant under-prediction of the lateral stiffness and capacity of monopiles. To overcome the shortcoming, the authors have previously proposed a conceptual two-spring framework, i.e., the so-called '*p-y* + M_R-θ_R' model, to capture the monopile response in soft clay under lateral loading. The framework uses distributed *p-y* springs to consider the lateral soil resistance along the pile above the rotation point (RP) and a single moment-rotation (M_R-θ_R) spring attached at the RP to capture the entire soil resistance below the RP, i.e., the distributed resistance along the pile, base shear and base moment at the pile tip. The proposed *p-y* and M_R-θ_R springs were curve-fitted to the results of 3D numerical analyses. However, as the stress-strain response and the shear strength profile inevitably influence the *p-y* and M_R-θ_R springs, the applicability of the empirical formulations to soil conditions other than those examined is uncertain. This study proposes an enhancement to the '*p-y* + M_R-θ_R' framework, in which the *p-y* and M_R-θ_R springs are not tied to a specific soil and strength profile but fundamentally linked to the properties that can be measured directly in the site investigation and laboratory. This extension is achieved through analytical analyses and an extensive parametric numerical study. The predictive capabilities of the model are demonstrated by back-analyses of finite element analyses and centrifuge model tests. The proposed model provides practising engineers with a simple yet powerful approach to use site-specific soil reaction curves in the design of monopiles embedded in soft clay.

1. Introduction

Monopiles are the dominant foundation solution for supporting offshore wind turbines (OWTs). To resist large lateral load and bending moment resulting from wind, waves and current, pile diameter (D) in the range of 6–8 m is common nowadays. Extra-large monopiles with diameter greater than 10 m are also being considered in newer projects. The embedded length-to-diameter ratio (L/D) of monopiles is typically in the range of 4–8 (Doherty and Gavin, 2012; Murphy et al., 2018) in competent soils. In soft seabed conditions, such as offshore China, the L/D ratio can be as high as 10 or more (Lai et al., 2020).

1.1. Literature review

Monopile foundations are commonly designed using the beam-column approach where the pile is modelled as an equivalent elastic beam and the lateral soil resistance are represented by distributed nonlinear *p-y* springs along the pile length. In soft clays, the API formulation (API Recommended Practice 2GEO, 2014) has been conventionally used, despite that the API *p-y* model is originally developed for the design of small diameter slender piles used in the offshore oil and gas industry. Direct adoption of the API model to the design of monopiles with small L/D ratios are insufficient and may lead to an underestimation of lateral pile capacity and stiffness (Gerolymos and Gazetas, 2006; Lam, 2009; Gao et al., 2015; Byrne et al., 2017, 2019; Wang et al., 2018, 2020; Zhang and Andersen, 2019; Fu et al., 2020a).

* Corresponding author.
E-mail addresses: yongqing_lai@zju.edu.cn (Y. Lai), wanglz@zju.edu.cn (L. Wang), youhu.zhang@ngi.no (Y. Zhang), yi_hong@zju.edu.cn (Y. Hong).

https://doi.org/10.1016/j.oceaneng.2020.108437
Received 10 May 2020; Received in revised form 2 October 2020; Accepted 29 November 2020
Available online 9 December 2020

During the past decade, a number of alternative *p-y* formulations have been proposed for improving the modelling of slender pile response in clay through numerical, analytical and experimental studies. Examples are, among others, Jeanjean (2009), Yu et al. (2017), Zhang and Andersen (2017), Jeanjean et al. (2017) and Zhu et al. (2017). It is worth noting that generalized approach proposed Zhang and Andersen (2017) and Jeanjean et al. (2017), which derives the site-specific *p-y* response by mapping the normalised stress-strain response measured in direct simple shear test is set to be incorporated in the upcoming revisions of the ISO 19901-4 and API RP2GEO and supersedes the existing clay *p-y* formulation.

To gain insight into the monopile response, a joint industry research project PISA performed a comprehensive set of large scale field tests on model piles. Based on the test results and extensive 3D finite element analyses, Byrne et al. (2017, 2019) emphasized that for monopiles, besides the distributed lateral soil resistance, additional resistance components including the base shear, the base moment and the distributed moment resistance due to vertical shaft friction are meaningful and cannot be neglected for optimized design. They proposed a four-spring model for monopile analysis, which includes the aforementioned soil resistances. Zhang and Andersen (2019) proposed a two-spring model that accounts for the distributed lateral soil resistance along the pile and the base shear at the pile tip, arguing that the base moment is negligible. Compared to the PISA model, Zhang and Andersen (2019) linked the soil springs to the elemental stress-strain response of the soil for ease of application in design. Fu et al. (2020a) further proposed scaling relationship for mapping stress-strain response to distributed moment-rotation spring due to the vertical shaft friction. In addition, three-dimensional numerical models are widely adopted in research for analysing monopile behaviour (Kim and Jeong 2011; Qi et al., 2014; Achmus and Thieken 2016; He et al., 2019; Wang et al., 2020), which are capable of modelling complex three-dimensional pile-soil interaction. However, it is clear that three-dimensional numerical modelling is too computationally expensive, and thus may not suitable for engineering practice (Burd et al., 2017).

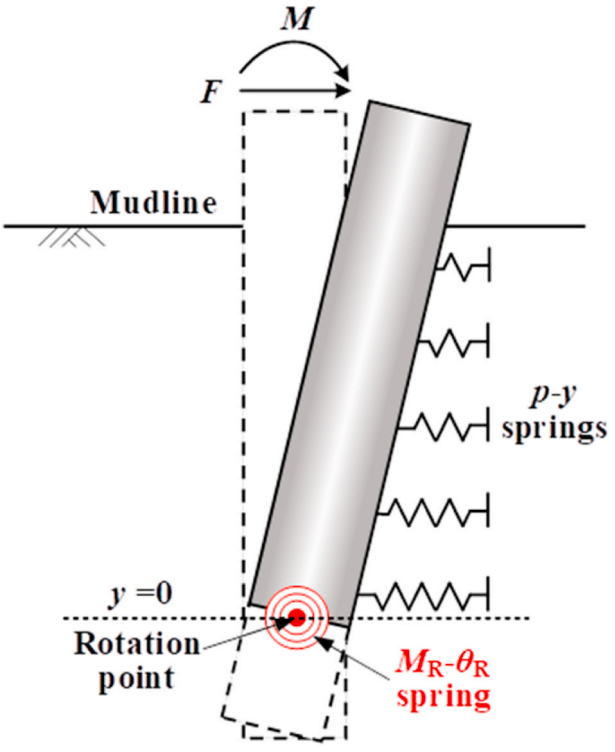

Fig. 1. '*p-y* + M_R-θ_R' conceptual framework proposed by Wang et al. (2020) for monopile analysis.

The authors have previously proposed a conceptual framework, termed as '*p-y* + M_R-θ_R' model (as illustrated in Fig. 1). The soil resistance along the pile above the rotation point (RP) is represented by distributed lateral springs (*p-y* springs), while the soil resistance below the rotation point is modelled by (i) constraining the lateral displacement at the rotation point, and (ii) incorporating a concentrated rotational spring (M_R-θ_R spring) at the rotation point. By doing so, the overall soil resistance at and below the rotation point, including the contributions from the base shear and base moment, are all integrated into the concentrated rotational spring. Validation exercises demonstrate that the model can predict the lateral behaviour of monopiles with a range of *L/D* ratios using a unified set of parameters (Wang et al., 2020).

Although the original '*p-y* + M_R-θ_R' framework is simple and easy to apply, the formulations of the *p-y* and the M_R-θ_R curves were based on empirical curve-fitting to the results of finite element analyses in a specific soil (normally consolidated Malaysian kaolin). It is well established that soil reaction curves are highly dependent on the stress-strain response of the soil (Bransby, 1999; Klar and Osman, 2008; Yu et al., 2017; Zhang and Andersen, 2017, 2019). A soil with stiffer stress-strain response will naturally result in stiffer soil reaction curves, and vice versa. In addition, the strength distribution below the rotation point will naturally changes the ultimate capacity of the M_R-θ_R curve. Based on the above discussions, the applicability of the previously proposed '*p-y* + M_R-θ_R' framework to other soil conditions is uncertain and further development is necessary to generalise the model for wider range of soil conditions.

1.2. Motivation of this study

The motivation of this study is therefore to enhance the previously proposed '*p-y* + M_R-θ_R' framework so that the formulations of the *p-y* and M_R-θ_R springs are no longer tied to a specific soil type and strength profile but linked to fundamental soil properties that can be directly measured in routine site investigation and laboratory testing. Note that Zhang and Andersen (2017) have already proposed a model for mapping the lateral *p-y* response in clay from the laboratory stress-strain curves (more details are provided in Section 5.1). Therefore, this study mainly focusses on the development of a model for the construction of the M_R-θ_R spring from the site-specific stress-strain response and the undrained shear strength profile.

Osman and Bolton (2005) proposed the so-called 'mobilizable strength design (MSD)' concept, which assumes self-similarity between the stress-strain response of a soil element and the load-displacement response of a boundary value problem. Based on this concept, the work by Osman et al. (2007) demonstrates that, for a circular surface foundation under pure moment loading, its moment-rotation response can be scaled from the soil element's stress-strain response. For monopiles, the M_R-θ_R response at the rotation point can be regarded as the moment-rotation response of an imaginary circular foundation, with embedment equal to the pile length below the rotation point. As the soil failure mechanism beneath the circular surface foundation is similar to that below the rotation point of a monopile, i.e., a rotational scoop-type mechanism (Hong et al., 2017). It is worth noting that in the current framework, the lumped M_R-θ_R response is only meant to capture the soil resistance below the rotation point. The soil that is above the rotation point but also mobilised by the rotational mechanism does indeed contribute to additional resistance. However, this resistance is captured by the distributed *p-y* springs. Based on the above discussion, it is possible and rationale to link the M_R-θ_R response of the monopiles to the stress-strain response of the soil.

In this study, an analytical derivation of the ultimate capacity of the M_R-θ_R spring based on the well-established scoop failure mechanism is first presented. Thereafter an extensive numerical parametric investigation of the M_R-θ_R responses for various geometries over a wide range of stress-strain behaviours and undrained shear strength profiles is

performed. The parametric investigation explores the scaling relationship of the M_R-θ_R springs to the stress-strain response and how that scaling relation is influenced by the strength profile and geometry. Lastly, to verify the validity of the proposed '*p-y* + M_R-θ_R' framework, pile responses computed by 3D finite element analyses and measured in centrifuge model tests are compared with the model predictions.

2. Analytical solution for ultimate moment capacity of M_R-θ_R curves (M_{R_ult})

As reported by Hong et al. (2017) and Zhang and Andersen (2019), for semi-rigid or rigid monopiles, the soil failure mechanism below the pile rotation point takes the form of a rotational scoop around the rotation point. Therefore, the upper-bound solution of the reacting ultimate moment capacity M_{R_ult} about the rotation point is given as the sum of the moment resistance due to the scoop failure surface (M_{R_scoop}) and side shear (M_{R_side}):

$$M_{R\_ult} = M_{R\_scoop} + M_{R\_side} \tag{1}$$

The scoop failure surface is a 3D surface. The ultimate moment resistance from the scoop failure surface M_{R_scoop} can be considered as the sum of the moment resistance from the slip surfaces caused by a series of strips, as illustrated in Fig. 2. A strip (AA′) with a thickness of *dy* and located at a distance *y* from the pile central cross-section forms a semi-circle slip surface CBB'C' with a radius of r_f:

$$r_f = O'B = \sqrt{(O'A')^2 + (A'B')^2} = \sqrt{(OA')^2 - (OO')^2 + (A'B')^2} = \sqrt{(\frac{D}{2})^2 - y^2 + H^2} \tag{2}$$

For a linearly increasing undrained shear strength profile with a strength at the rotation point equal to s_{u0} and a strength gradient *k* (see Fig. 2), the moment resistance about the rotation point (*O*′) due to the slip surface caused by strip AA′ can be calculated as (assuming unit thickness, i.e., $dy = 1$):

$$M_{R\_scoop-section} = 2\int_0^{\frac{\pi}{2}} (s_{u0} + kr_f \sin\alpha)\cdot r_f \cdot (dl \cdot 1) = 2\int_0^{\frac{\pi}{2}} (s_{u0} + kr_f \sin\alpha)\cdot r_f \cdot r_f \cdot d\alpha \tag{3}$$

Therefore, the M_{R_scoop} due to the 3D scoop failure surface is:

$$M_{R\_scoop} = 2\int_0^{\frac{D}{2}} \cdot M_{R\_scoop-section}\ dy \tag{4}$$

Substituting Eq. (3) into Eq. (4):

$$M_{R\_scoop} = 2\int_0^{\frac{D}{2}} \cdot 2\int_0^{\frac{\pi}{2}} (s_{u0} + kr_f \sin\alpha)\cdot r_f \cdot r_f \cdot d\alpha \cdot dy = (\frac{1}{6}\pi D^3 s_{u0} + \pi s_{u0} D H^2) + k(\frac{1}{2}D^2 + 2H^2)^2[\frac{3}{8}t + \frac{1}{4}\sin(2t) + \frac{1}{32}\sin(4t)] \tag{5}$$

where $t = \arcsin(\frac{D}{\sqrt{D^2+4H^2}})$.

Due to the circular cross-section of the monopile, a 3D spherical scoop mechanism is mobilised by the pile around the rotation point. It was not attempted to derive the moment resistance due to side shear directly. Instead, the resistance for a square cross-section is first derived and then corrected for the shape by applying a side shear factor which is well established for suction anchor design at NGI (Jostad and Andersen, 2015). Assuming a square pile cross-section with the width equal to the pile diameter *D*, the ultimate moment resistance contributed from the shear on the two side planes(M_{R_side}) is given as the sum of reacting moment about axis *E-E'* (as shown in Fig. 3):

$$M_{R\_side} = 2\int_0^H 2\int_0^{\frac{\pi}{2}} (s_{u0} + kz\sin\delta)\cdot z \cdot dl \cdot dz = 2\int_0^H 2\int_0^{\frac{\pi}{2}} (s_{u0} + kz\sin\delta)\cdot z \cdot z \cdot d\delta \cdot dz \tag{6}$$

However, the monopile foundation has a circular cross-section instead of a square. The difference in shape results in a reduced side shear resistance which is corrected by a side shear factor r_{ss}. For computing the holding capacity of suction anchors using 2D soil elements, Jostad and Andersen (2015) carried out series of comparative 2D and 3D finite element analyses on suction anchors of different length to diameter ratios in order to calibrate the side shear factor which accounts for the 3D shape of the suction anchor. They concluded a side shear factor $r_{ss} = 0.73$ for correcting for the 3D effect. Therefore, $r_{ss} = 0.73$ is applied herein to correct the side shear moment resistance derived for a square cross-section:

$$M_{R\_side} = 2\int_0^H 2\int_0^{\frac{\pi}{2}} r_{ss}(s_{u0} + kz\sin\delta)\cdot z \cdot z \cdot d\delta \cdot dz = 0.73(\frac{2\pi}{3}s_{u0}H^3 + kH^4) \tag{7}$$

Therefore, substituting Eq. (5) and Eq. (7) into Eq. (1), the solution for ultimate moment capacity M_{R_ult} is:

$$M_{R\_ult} = (\frac{1}{6}\pi D^3 s_{u0} + \pi s_{u0} D H^2) + k(\frac{1}{2}D^2 + 2H^2)^2[\frac{3}{8}t + \frac{1}{4}\sin(2t) + \frac{1}{32}\sin(4t)] + 0.73(\frac{2\pi}{3}s_{u0}H^3 + kH^4) \tag{8}$$

where $t = \arcsin(\frac{D}{\sqrt{D^2+4H^2}})$.

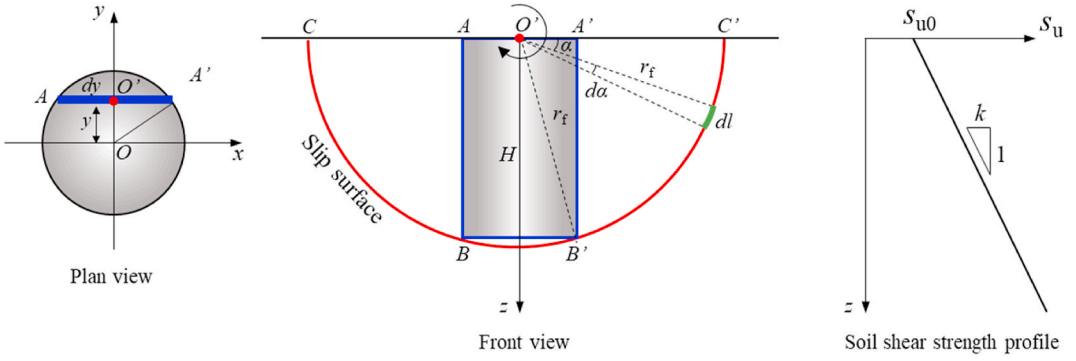

Fig. 2. Schematic illustration for calculating the moment resistance from the scoop failure surface (M_{scoop}).

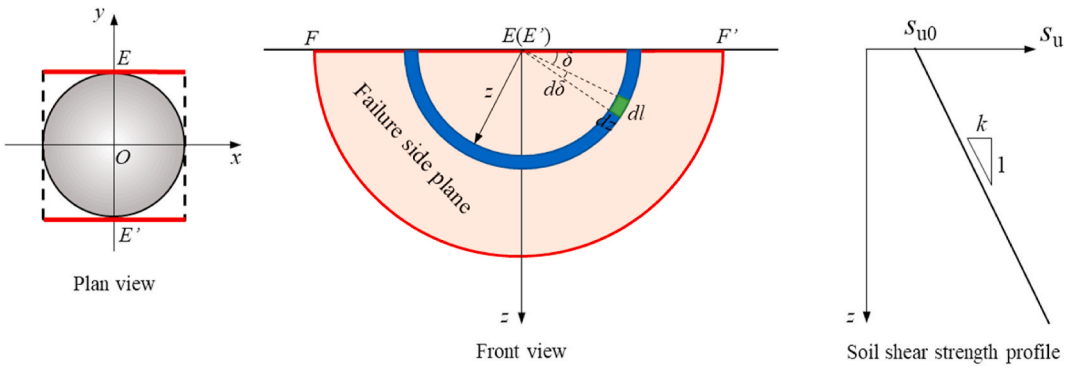

Fig. 3. Schematic illustration for calculating the moment resistance from the side shear (M_{R_side}).

3. M_R-θ_r response of monopiles in soft clay: methodology of 3D numerical parametric study

3.1. Simplified finite element model to investigate M_R-θ_R response of monopiles

To form the 'p-y + M_R-θ_R' model, the M_R-θ_R spring, as a key element of the model, should be generalized. To formulate M_R-θ_R response of monopiles, Wang et al. (2020) performed a series of numerical analyses of full-length monopiles with various L/D ratios. The pile bending moment and rotation at the rotation point was extracted to form the M_R-θ_R curves. In this study, a more efficient method is adopted. Instead of modelling the full-length monopile, only the monopile below the rotation point is modelled since the M_R-θ_R response represents the overall soil resistance below the rotation point, as illustrated in Fig. 4. It should be borne in mind that the M_R-θ_R response is only meant to capture the soil resistance below the rotation point. The soil resistance above the rotation point is captured by the distributed p-y springs in the current framework. Lateral displacement at the rotation point is constrained and a pure moment loading is applied on the top surface of the pile model, enforcing a rotational scoop mechanism around the rotation point. By doing so, the behaviour of the monopile below the rotation point is reproduced by the simplified model. The computed moment-rotation response of the pile model equivalents to the M_R-θ_R response below the RP of a monopile. The validity of the simplified approach is examined in Section 3.4 where the M_R-θ_R responses computed by the simplified models are compared with those extracted from the full-length monopile models.

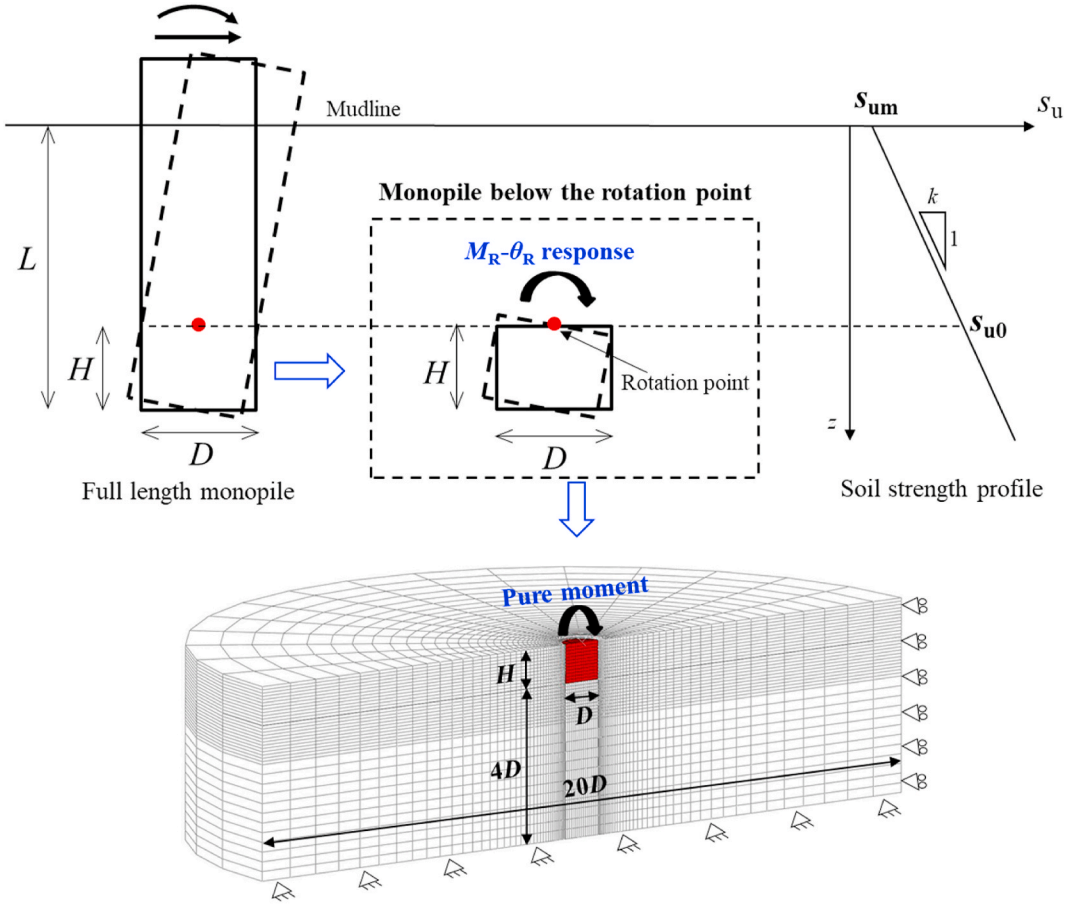

Fig. 4. Typical three-dimensional finite element mesh for investigating the M_R-θ_R response of pile below the rotation point (simplified model).

The numerical analyses were performed in ABAQUS (Abaqus, 2014). This study considers a monopile with a diameter (D) of 6 m and a range of pile lengths (H) below the rotation point. $H = 3$, 6, 9, 12 and 15 m are considered, covering H/D ratios from 0.5 to 2.5, which is considered a practical range. As the results will be presented in a normalised format, the absolute dimension of the pile diameter does not matter. A typical three-dimensional finite element mesh for a monopile with $D = 6$ m and $H = 6$ m is illustrated in Fig. 4. Only half of the pile is modelled by taking advantage of the symmetry. The diameter of the cylindrical soil block and the distance between the pile tip and the soil bottom boundary are chosen to be 20D and 5D, respectively, to minimize the boundary effect. The lateral boundary of the finite element mesh is constrained by roller support while the bottom boundary is fixed by pinned support. The top of the soil domain is set free to displacement.

The monopile is constrained to be a rigid body for simplicity, which is considered reasonable since the pile rotates with negligible bending below the rotation point. A fully rough pile-soil interface is modelled in the numerical analyses. On the front side of the loading direction, the pile pushes against the soil above the rotation point, thus cutting off the water flow path if a tension gap was to open below the rotation point. On the rear side, the pile kicks against the soil below the rotation point. Thus, no separation is allowed on the interface. A pure moment load is applied on the top surface of the pile and the ultimate state is indicated by minimal increase in moment load with increase of rotation.

3.2. Soil model

The soil is described by a total stress, anisotropic model: NGI-ADP model (Grimstad et al., 2012). For simplicity, the strength and stiffness anisotropy are not considered. Although the NGI-ADP model is not a built-in soil model in ABAQUS, it was achieved by adopting the Mohr-Coulomb model with a zero-degree friction angle (i.e., Tresca yield criterion) and specifying a table of plastic shear strain versus yield stress (i.e., mobilised shear stress). In this study, the stress-strain response (plastic component) is calculated using the following plastic hardening rule adopted by the NGI-ADP model and then used as input in ABAQUS.

$$\frac{\tau}{s_u} = 2\frac{\sqrt{\gamma^p / \gamma_f^p}}{1 + \gamma^p / \gamma_f^p} \tag{9}$$

where τ = currently mobilised shear stress; s_u = the shear strength of soil; γ^p = the current plastic shear strain; γ_f^p = the plastic shear strain at failure (full mobilisation). The total shear strain γ associated with the currently mobilised shear stress τ is the summation of elastic and plastic shear strain components (γ^e and γ^p respectively):

$$\gamma = \gamma^e + \gamma^p = \frac{\tau}{G_{max}} + \gamma^p = \frac{\tau / s_u}{G_{max}/s_u} + \gamma^p \tag{10}$$

where G_{max}/s_u is the small strain shear modulus ratio and is used to calculate the elastic component of shear strain over the entire stress range.

As can be seen from Eqs. (9) and (10), the NGI-ADP model uses two parameters, i.e., γ_f^p and G_{max}/s_u, to define the stress-strain response of clay. G_{max} can be determined through a resonant column test or bender elements incorporated in a soil element test. γ_f^p literally stands for the plastic shear strain at failure and should be determined by curve-fitting that provides the best fit to the stress-strain curve measured in the soil element shear test. Zhang and Andersen (2017) demonstrate that the model can describe the stress-strain behaviour measured over a wide range of natural clays with combinations of the two parameters.

3.3. Parametric range

In this study, an extensive numerical parametric study over a wide range of H/D ratios and soil stress-strain response is carried out to investigate the M_R-θ_R response. The ranges of the parameters are summarized in Table 1.

It is assumed that the part of the pile below the rotation point is embedded entirely within a single soil layer with a constant or linearly increasing strength profile and the degree of soil strength heterogeneity can be expressed by the normalised parameter κ, defined as:

$$\kappa = \frac{kD}{s_{u0}} \tag{11}$$

where k and s_{u0} denote the shear-strength gradient and the shear strength at the depth of the rotation point, respectively, as illustrated in Fig. 4. In this study, a pile diameter of $D = 6$ m is fixed, while a range of soil strength profiles are investigated. They are detailed in Table 2, which presents a normalised group κ varying from 0 to 0.5.

In total, 300 3D finite element analyses involving the full combination of all parameters listed in Tables 1 and 2 are performed, producing 300 M_R-θ_R curves. The scaling relationship between the M_R-θ_R curve and the corresponding soil stress-strain curve is explored, which will be presented below.

3.4. Validation of the simplified finite element model for investigating M_R-θ_R response

Before performing the numerical parametric study using the simplified finite element model, the validity and accuracy of the simplified model for deriving M_R-θ_R response is verified first. For this purpose, the M_R-θ_R responses computed by the simplified model are compared with those computed by the corresponding full length monopile model.

Two finite element analyses of laterally loaded full length monopiles with a diameter $D = 6$ m with L/D ratio of 4 and 5 are carried out. The monopiles are modelled as linearly elastic solid cylinders, assigned with equivalent elastic properties that produce bending stiffness (EI) that is equivalent to the steel hollow piles with a wall thickness of 0.06 m. Typical finite element mesh for the full length monopile with $L/D = 5$ is presented in Fig. 5. The pile stick-up above the soil surface is kept 30 m for the two L/D ratios, where a lateral force is applied. The magnitude of the applied lateral force does not matter as long as the full M_R-θ_R response can be obtained from the numerical results. Therefore, in the analyses reported herein, a relatively large lateral force is applied to ensure the M_R-θ_R response reaches its ultimate state, i.e., the M_R-θ_R curve reaches a plateau. The soil is described by the NGI-ADP model (see Section 3.2) with parameters of $\gamma_f^p = 5\%$ and $G_{max}/s_u = 500$. An effective soil unit weight of 6 kN/m^3 is adopted for all the cases. The soil strength increases linearly with depth at a gradient of 1.5 kPa per metre, i.e., $s_u = 1.5z$. A fully rough pile-soil interface is modelled and separation between the interface is not allowed.

The pile bending moment (M_R) and rotation angle (θ_R) at the depth of the rotation point were extracted from the full length monopile model to form the M_R-θ_R relationships. The length of the pile below the rotation point (H) is also obtained from the finite element analyses. Based on the H revealed by the full-length models, corresponding simplified finite

Table 1
Range of parameters considered in this finite element parametric analyses.

Parameter	Value
H/D	0.5, 1, 1.5, 2, 2.5
γ_f^p (%)	2, 5, 10, 15
G_{max}/s_u	250, 500, 1000
κ	0, 0.05, 0.1, 0.2, 0.5

Table 2
Soil profiles considered in this study.

Parameters	Soil profile				
	1	2	3	4	5
s_{u0} (kPa)	100	144	96	60	30
k (kPa/m)	0	1.2	1.6	2	2.5
$\kappa=kD/s_{u0}$	0	0.05	0.1	0.2	0.5

element models, in which only the monopile below the rotation point is modelled (as illustrated in Fig. 4), are then developed for deriving the M_R-θ_R responses using the simplified approach as presented in Section 3.1. The computed M_R-θ_R responses from the simplified finite element models are compared with those computed from the full-length model in Fig. 6. It can be seen from the figure that, the M_R-θ_R responses computed by the simplified models match well with those computed by the full-length monopile models, demonstrating the validity and accuracy of the simplified model. Fundamentally the good match is obtained because: i) undrained soil response is assumed here thus the soil weight above the rotation point does not affect the undrained shear strength of the soil below the rotation point; ii) since a pure rotational scoop mechanism is enforced about the rotation point, the soil mechanism below the rotation point is the same with or without the soil above it. The mobilised resistance offered by the soil below the rotation point is thus the same with or without soil above the rotation point.

It should be reiterated that the lumped M_R-θ_R is only meant to capture the soil resistance below the rotation point. The soil that is above the rotation point but also mobilised by the rotational mechanism does indeed contribute to additional resistance. However, this contribution is captured by distributed p-y springs in the current framework.

4. Numerical analysis results

4.1. Ultimate moment capacity of M_R-θ_R curves (M_{R_ult})

Fig. 7 shows the variation of the computed ultimate moment capacity (M_{R_ult}) with soil-strength heterogeneity (κ) and H/D ratio. In the figure, M_{R_ult} is normalised by ADs_{u0}, where A is the overall cross-sectional area enclosed by the pile.

As expected, M_{R_ult} is strongly influenced by κ and the H/D ratio. At any given of H/D ratio, M_{R_ult} shows an approximately linear relationship with soil-strength heterogeneity κ. Comparing to the influence of κ, the increase in H/D ratio leads to a much more pronounced growth in M_{R_ult}. As illustrated in Fig. 7, the M_{R_ult} is well predicted by the analytical solution presented in Section 2.

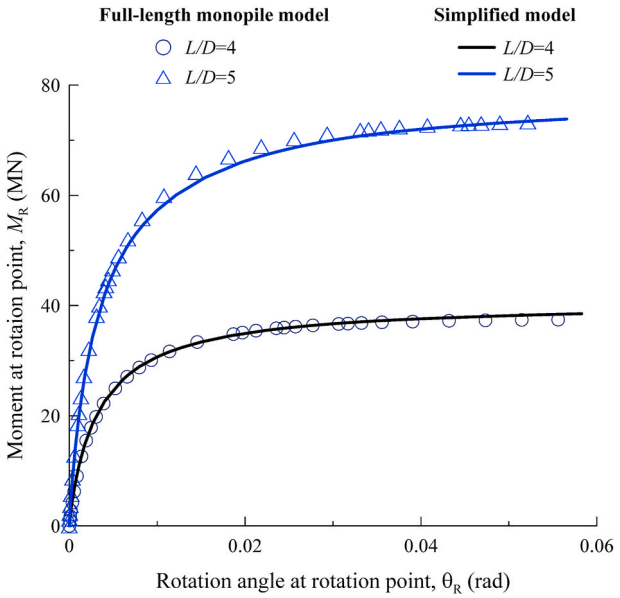

Fig. 6. Comparison of M_R-θ_R responses computed by the simplified model (modelling monopile below the rotation point) and full-length monopile model.

4.2. Normalised M_R-θ_R curves

Fig. 8(a)-8(d) presents some typical results, illustrating the influence of H/D ratio, γ_f^p, G_{max}/s_u and κ on the normalised M_R-θ_R curves (M_R/M_{R_ult} vs θ_R), respectively. The representative set of M_R-θ_R curves presented in Fig. 8(a) shows that as the H/D ratio increases, the normalised M_R-θ_R curve becomes gradually softer. This is as expected that when H/D ratio increases, the rotational soil scoop expands and thus a larger rotation angle (θ_R) is needed to reach failure, resulting in a softer

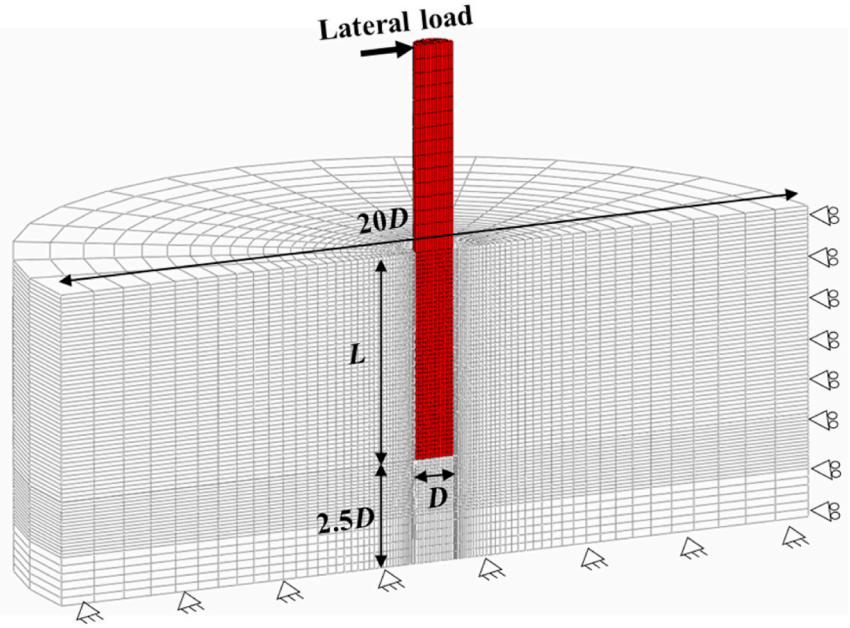

Fig. 5. Typical three-dimensional finite element mesh of a full length monopile.

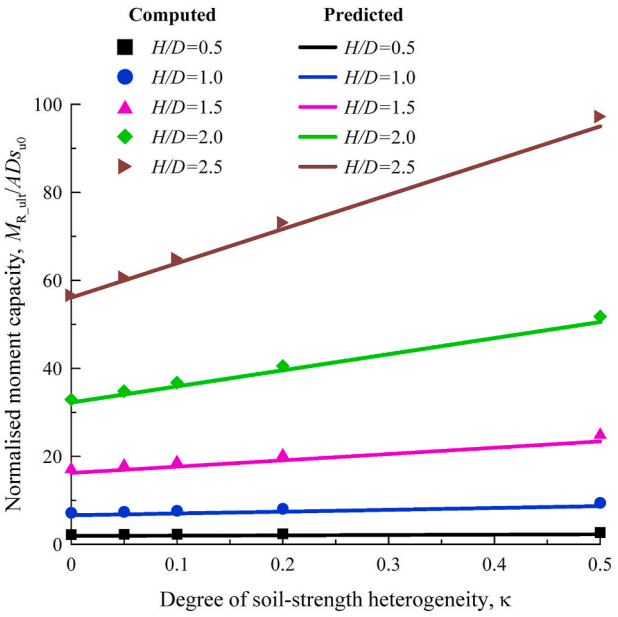

Fig. 7. Comparison between computed and predicted ultimate moment capacity (M_{R_ult}) of the M_R-θ_R curves.

response. Fig. 8(b) presents an example set of four computed M_R-θ_R curves for four soil stress-strain responses that are increasingly softer (i.e., $\gamma_f^p = 2, 5, 10, 15\%$). As anticipated, the computed M_R-θ_R response also becomes increasing softer. Different from the H/D ratio and γ_f^p, G_{max}/s_u and κ exhibit negligible impact on the normalised M_R-θ_R curves, as can be seen in Fig. 8(c) and (d), respectively.

From Fig. 8, it is clear that the shape of the M_R-θ_R curves bears strong similarities to the soil stress-strain curves that were used as input to derive them. Therefore, it is interesting to explore the possibility of "scaling" the soil stress-strain curves to the M_R-θ_R curves, which is attempted in the following section.

5. Proposed site-specific '*p-y* + M_R-θ_R' framework

This section aims to propose a site specific '*p-y* + M_R-θ_R' framework, where the *p-y* and M_R-θ_R curves can be constructed by directly scaling the soil stress-strain curves measured in the laboratory tests. While the site-specific *p-y* curves proposed by Zhang and Andersen (2017) is adopted for capturing the soil resistance above the rotation point, attempt is made in this section to link the M_R-θ_R curves to the soil stress-strain curves based on the results of the extensive parametric numerical analyses.

5.1. *p-y* curves

Based on an extensive finite element study, Zhang and Andersen (2017) proposed a framework that allows for construction of site-specific *p-y* curves by directly scaling the soil stress-strain curves measured in laboratory element test, as schematically illustrated in Fig. 9. A point on the stress-strain curve with mobilisation in shear stress (τ/s_u) corresponds to a point on the *p-y* curve with the same level of mobilisation in lateral bearing pressure (p/p_u):

$$\frac{p}{p_u} = \frac{\tau}{s_u} \tag{12}$$

The corresponding normalised lateral displacement (y/D) can be scaled from the shear strain (γ) by using two scaling factors:

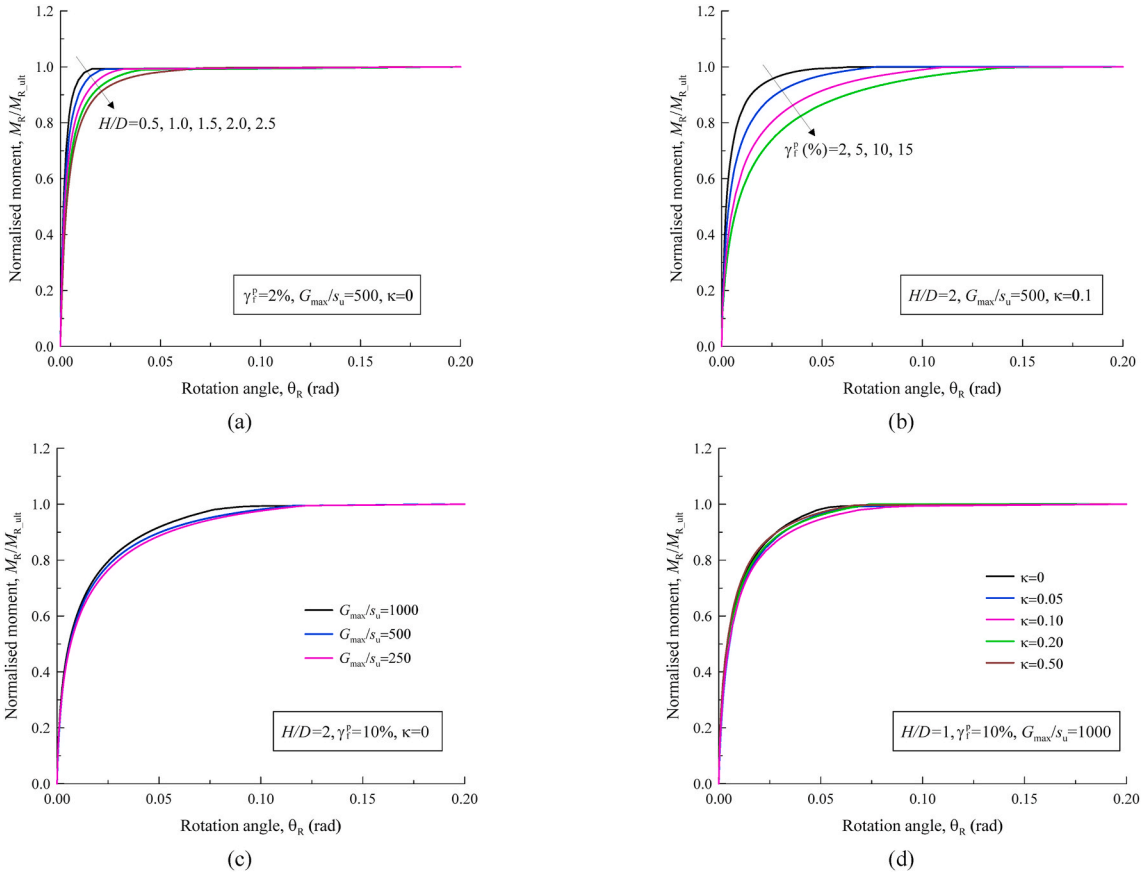

Fig. 8. Example finite element analyses results showing the influence of (a) H/D ratio, (b) γ_f^p, (c) G_{max}/s_u, and (d) κ on normalised M_R-θ_R curves.

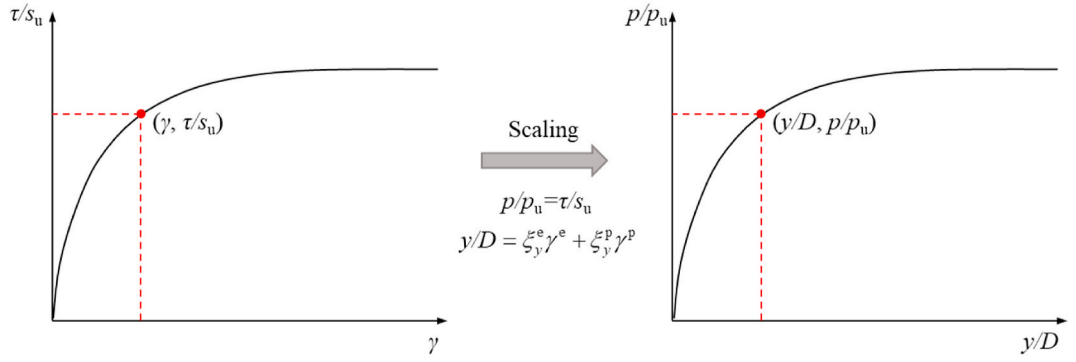

Fig. 9. Schematic illustration of scaling *p-y* curve from stress-strain curve (Zhang and Andersen, 2017).

$$\frac{y}{D}=\xi_y^e\gamma^e+\xi_y^p\gamma^p \tag{13}$$

$$\gamma^e=\frac{\tau}{G_{max}}=\frac{\tau/s_u}{G_{max}/s_u} \tag{14}$$

$$\gamma^p=\gamma-\gamma^e \tag{15}$$

where ξ_y^e and ξ_y^p are the two scaling factors applied to the elastic and plastic components of the shear strain, respectively. For simplicity, a constant value of $\xi_y^e=2.8$ is proposed, while ξ_y^p is expressed as a function of pile-soil interface roughness factor (α): $\xi_y^p=1.35+0.25\alpha$. Further details on the derivation of the scaling factors can be found in Zhang and Andersen (2017).

It should be noted that this *p-y* framework is strictly only applicable for a plain strain flow-around soil mechanism, and thus it is more suitable for flexible piles. For a rigid or semi-rigid monopile, the soil flow mechanisms are dominated by a wedge-type flow in the upper part and a rotational flow in the lower part (Hong et al., 2017). Considering the soft clay conditions concerned in this paper, a tension gap is unlikely on the rear side of the monopile (Fu et al., 2020b), and thus two soil wedges (passive and active wedge) will be mobilised. This is not too dis-similar to the condition of a flow-around mechanism. Therefore, despite the difference in soil mechanisms, the *p-y* curves proposed by Zhang and Andersen (2017) are recommended for representing the lateral soil resistance above the rotation point. The suitability of the *p-y* curves will be examined later when the proposed model is used to back-analyse the pile response obtained from centrifuge tests and finite element analyses.

Through Eqs. 12–15, the shape of the *p-y* curves (p/p_u vs y/D) is determined. The ultimate soil resistance of the *p-y* curves (p_u) is calculated by:

$$p_u=N_p s_u D \tag{16}$$

where N_p is the lateral bearing capacity factor. For the condition with suction (i.e., no tension gap), the equations proposed by Zhang et al. (2016), which is derived from Yu et al. (2015)'s upper bound analyses, is adopted in the model to calculate the N_p value, as follows:

$$N_p=2[N_1-(N_1-N_2)\frac{z/D}{d})(\frac{z/D}{d})(\frac{z/D}{d})^{0.6})^{1.35}-(1-\alpha)]\le N_{pd} \tag{17}$$

$$N_{pd}=9.14+2.8\alpha \tag{18}$$

where $N_1=11.94$; $N_2=3.22$; $d=16.8–2.3\log_{10}(\lambda)$, $\lambda=s_{um}/kD$ and $0.1\le\lambda\le10$, s_{um} is the soil shear strength at the mudline, as shown in Fig. 4.

5.2. M_R-θ_R curves

Due to the similarities between the input soil stress-strain curves and derived M_R-θ_R curves, a simple scaling model similar to the *p-y* model is proposed, as illustrated in Fig. 10. A point on the stress-strain curve with mobilisation in shear stress (τ/s_u) corresponds to a point on the M_R-θ_R curve with the same level of mobilisation in moment resistance (M_R/M_{R_ult}):

$$\frac{M_R}{M_{R\_ult}}=\frac{\tau}{s_u} \tag{19}$$

The corresponding normalised rotation angle (θ_R) can be scaled from the shear strain (γ) by using two scaling factors:

$$\theta_R=\xi_\theta^e\gamma^e+\xi_\theta^p\gamma^p \tag{20}$$

where ξ_θ^e and ξ_θ^p are the two scaling factors applied to the elastic and plastic components of the shear strain, respectively. γ^e and γ^p can be calculated by using Eqs. (14) and (15).

In elastic homogeneous soil ($k=0$ and $\kappa=0$) with constant shear modulus G, $\gamma^p=0$ and thus $\gamma=\gamma^e$. Eq. (19) can then be re-written as:

$$\frac{K_R(\xi_\theta^e\gamma)}{M_{R\_ult}}=\frac{G\gamma}{s_{u0}} \tag{21}$$

where K_R is elastic rotational stiffness. The elastic scaling factor ξ_θ^e follows that:

$$\xi_\theta^e=\frac{M_{R\_ult}G}{s_u K_R} \tag{22}$$

The closed-form solution of K_R for a rigid caisson (similar to the monopile segment below the rotation point) in elastic homogeneous soil has been proposed by Efthymiou and Gazetas (2019), which can be expressed by the following equation (assuming infinite bottom boundary):

$$K_R=\frac{GD^3}{3(1-\nu)}[1+1.5\frac{H}{D}(1+\frac{2H}{D})^{1.4}] \tag{23}$$

where ν is soil Poisson's ratio ($\nu=0.5$ for undrained condition).

According to Eq. (8), the M_{R_ult} for monopiles in homogenous soil with fully rough interface, i.e., $k=0$ and $\kappa=0$, can be expressed as:

$$M_{R\_ult}=(\frac{1}{6}\pi D^3 s_{u0}+\pi s_{u0}DH^2)+0.73(\frac{2\pi}{3}s_{u0}H^3) \tag{24}$$

Substituting Eqs. 23 and 24 into Eq. (22) leads to:

$$\xi_\theta^e=\frac{\pi}{4}[\frac{1+6(\frac{H}{D})^2+2.92(\frac{H}{D})^3}{(1+1.5\frac{H}{D}(1+\frac{2H}{D})^{1.4})}] \tag{25}$$

As illustrated in the equation, the ξ_θ^e is not a constant, but changes with H/D ratio. The variation of ξ_θ^e with H/D ratio according to Eq. (25) is presented in Fig. 11. For simplicity, the variation of ξ_θ^e is fitted by a linear equation:

$$\xi_\theta^e=0.63+0.32(\frac{H}{D}) \tag{26}$$

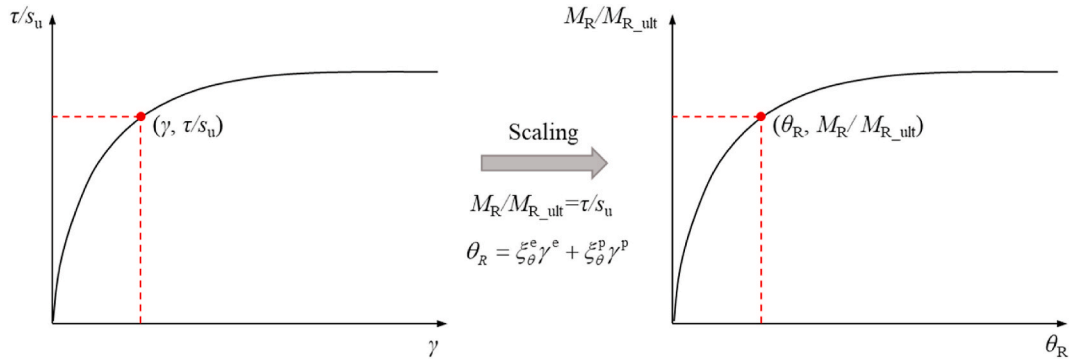

Fig. 10. Schematic illustration of scaling M_R-θ_R curve from stress-strain curve.

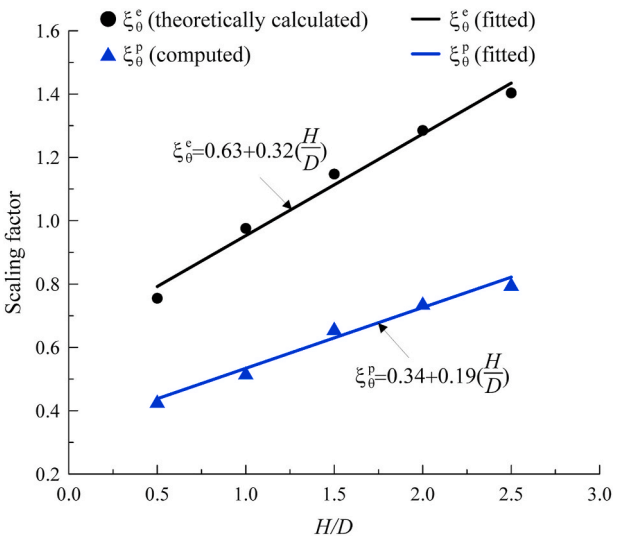

Fig. 11. Variation of the scaling factors with the H/D ratio.

It is worth noting that Eq. (26) for elastic scaling factor ξ^e_θ is derived for monopiles in homogenous soil ($\kappa = 0$). However, from the computed results presented in Fig. 8(d), the M_R-θ_R curves are insensitive to the degree of soil-strength heterogeneity κ. Therefore, the equation for ξ^e_θ is considered also applicable for monopiles in non-homogenous soil conditions.

Differing from the elastic scaling factor ξ^e_θ, the plastic scaling factor ξ^p_θ is developed based on the numerical results. A ξ^p_θ that varies linearly with H/D ratio is found to give a best fit to the numerical results based on least squares regressions:

$$\xi^p_\theta = 0.34 + 0.19\left(\frac{H}{D}\right) \tag{27}$$

The variation of ξ^p_θ is also presented in Fig. 11.

Fig. 12 shows an example where the M_R-θ_R curves constructed by the proposed approach (Eqs. 19 and 20 and (26)–(27)) for the same stress-strain curve are compared with those computed by the finite element analyses. Overall, a very good match is demonstrated between the finite element results and the model predictions for all H/D ratios examined here. As the H/D ratio increases (noting that the normalised M_R-θ_R response is insensitive to κ, as demonstrated in Section 4.2), the rotation needed to reach the ultimate moment resistance is increased, which amplifies the discrepancy towards higher mobilisation levels. In practice, the L/D ratio of offshore monopiles is typically in the range of 4–8 (Doherty and Gavin, 2012; Murphy et al., 2018). The pile length below the rotation point H varies between 0.2L-0.3L considering the depth of rotation point usually occurs between 0.7 and 0.8L (Chortis et al., 2020; Randolph and Gourvenec, 2011; Wang et al., 2020). This leads H/D ranges from 0.8 to 2.4, which is fully covered in this study. Therefore, it can be expected that the proposed approach is sufficiently accurate for analysing offshore monopiles. The stress-strain response of the soil layer below the rotation point measured at the in-situ stress state should be used for the mapping. The assumption is that the normalised stress-strain response remains relatively constant within the soil layer below the rotation point.

5.3. Determination of the depth of the rotation point

The above sections have described the proposed site-specific 'p-y + M_R-θ_R' model in detail, where the site-specific p-y and M_R-θ_R springs can be directly derived from soil stress-strain response measured in laboratory tests. In addition to the soil reaction curves, another key element of the proposed model is the depth of the rotation point.

For offshore monopiles in clay, as reported by Randolph and Gourvenec (2011) and Wang et al. (2020), the depth of the pile rotation point falls within $z = 0.75$–$0.80L$. Recently, Chortis et al. (2020) performed a series of high-quality centrifuge tests and three-dimensional finite element analyses, aiming to quantify the influence of scour depth and type on the lateral response of monopiles in sand. It is revealed by both centrifuge tests and numerical analyses that the pile rotation point occurs at 0.7L, irrespective of the magnitude of lateral displacement. Given the relatively narrow band (0.7–0.8L) for the depth of the rotation point, Wang et al. (2020) recommend a rotation point depth of $z = 0.80L$ for a quick assessment of the monopile response in the tender design and early design phases. For the detailed design, it is recommended to perform a trial analysis where p-y springs are used along the entire pile length. From the trial analysis, the depth of the rotation point can be well determined. As pointed out by Zhang and Andersen (2019), the depth of the rotation point is relatively insensitive to the p-y curves adopted. Therefore, a trial prediction is sufficiently accurate.

5.4. Summary of the proposed site-specific 'p-y + M_R-θ_R' model

Table 3 provides a summary of the proposed site-specific 'p-y + M_R-θ_R' model. Note that the proposed model is suited for different design limit states. It can be either used to check the bearing capacity of the pile under ultimate limit state (ULS) or the foundation stiffness for fatigue limit state (FLS) design. The spring components of the proposed model (p-y and M_R-θ_R) are formulated in such a way that the complete soil-pile interaction from initial stiffness at small displacement to degraded stiffness at large displacement is captured. The input to the model, i.e., strength and stress-strain response of the soil, should be aligned with the purpose of the springs.

6. Validation of the proposed site-specific 'p-y + M_R-θ_R' model

This section presents validation to the predictive capability of the site-specific 'p-y + M_R-θ_R' model against finite element analyses and

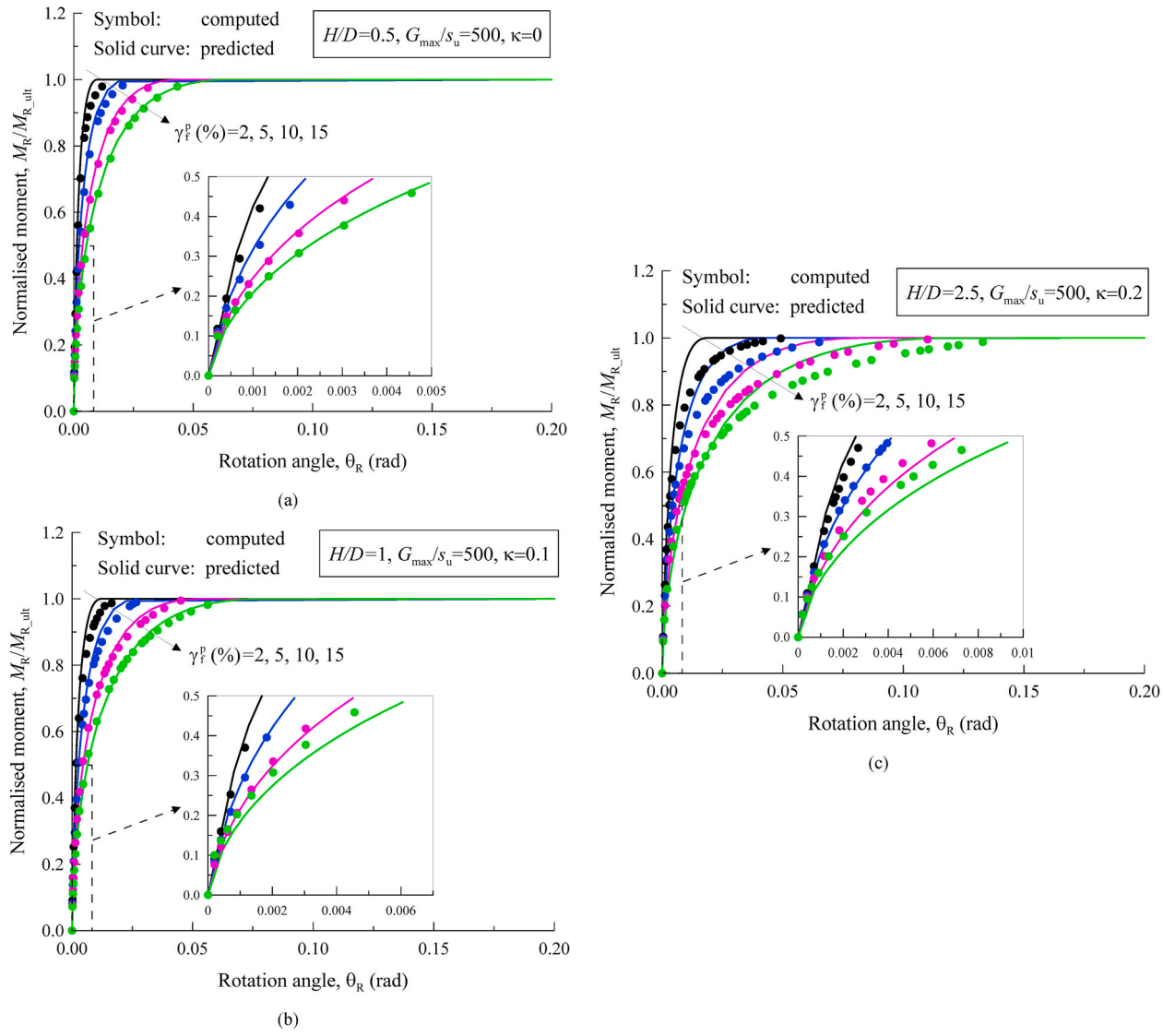

Fig. 12. Comparison of predicted M_R-θ_R curves against numerical results: (a) $H/D = 0.5$, $G_{max}/s_u = 500$, $\kappa = 0$; (b) $H/D = 1$, $G_{max}/s_u = 500$, $\kappa = 0.1$; (c) $H/D = 2.5$, $G_{max}/s_u = 500$, $\kappa = 0.2$.

published centrifuge pile test results. Comparisons between the computed/measured and predicted results are presented and discussed in the following subsections. The pile responses calculated by the API *p-y* curves are also included. When using the API curves, two input parameters, i.e., J and ϵ_{50}, should be determined. J is a dimensionless empirical factor that describes the rate of increase of the lateral bearing capacity factor N_p with normalised depth and ϵ_{50} denotes the axial strain at which 50% deviator stress is mobilised in an undrained compression test. In the following validation cases, a constant value of $J = 0.5$ is adopted, which is recommended by (Matlock (1970)) for normally consolidated soft clay. The value of ϵ_{50} is determined from the stress-strain curves of the corresponding soil.

6.1. *Validation against 3D finite element analyses of full-length monopiles*

To demonstrate the capability of the proposed model, finite element analyses of full-length monopiles with various L/D ratios and soil stress-strain responses are carried out. The diameter (D) and wall thickness (t) of the monopiles are fixed to 8 m and 0.09 m, respectively. Three pile embedment lengths of 24 m ($L/D = 3$), 32 m ($L/D = 4$) and 40 m ($L/D = 5$) are examined. A constant stick-up of 30 m is considered in all analyses. The undrained shear strength profile is $s_u = 5 + 1.5z$. The soil is modelled by the NGI-ADP model as described in Section 3.2, with the relevant parameters being: $G_{max/su} = 500$, and $\gamma_f^p = 5$, 8 or 10%. The fully rough interface between pile and soil is modelled, and tension gap on the soil-pile interface is not allowed.

Fig. 13 shows the comparison between computed and model predicted load-displacement relationship for three selected cases. As illustrated, the proposed model satisfactorily captures the computed pile responses by finite element analyses with different combinations of L/D ratio and stress-strain response. The model predicted pile responses are slightly softer than the computed responses by finite element analyses, which can be attributed to the neglect of the soil resistance contribution from the vertical pile shaft friction above the rotation point. The model predictions are considered sufficiently accurate for practical design purposes. Using the API *p-y* curves alone leads to much softer pile responses compared to the current model prediction which is due to: i) too soft distributed *p-y* curves, which has been discussed amongst others by Jeanjean (2009) and Zhang and Andersen (2017); ii) neglect of the soil resistance from the pile tip, which is more important for piles with smaller L/D ratios. In addition to the pile head load-displacement response, the proposed model also offers reasonable predictions for the displacement and rotation profiles, as illustrated in Fig. 14 for example.

Table 3
Summary of the site-specific 'p-y + M_R-θ_R' framework for monopile analysis.

Model	Description
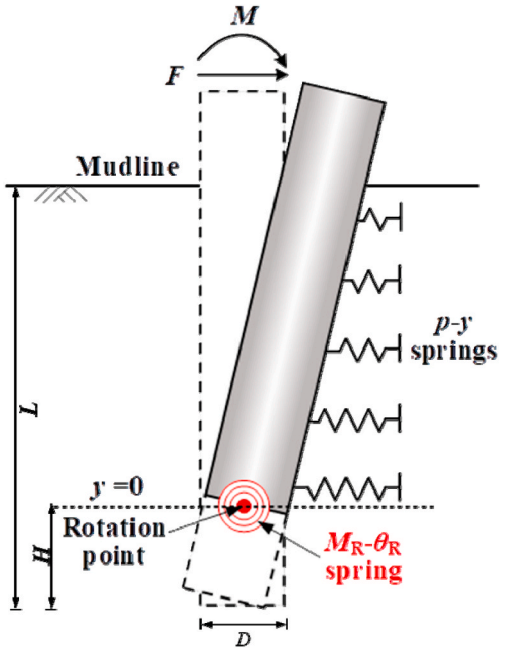	**Site-specific p-y curves:** 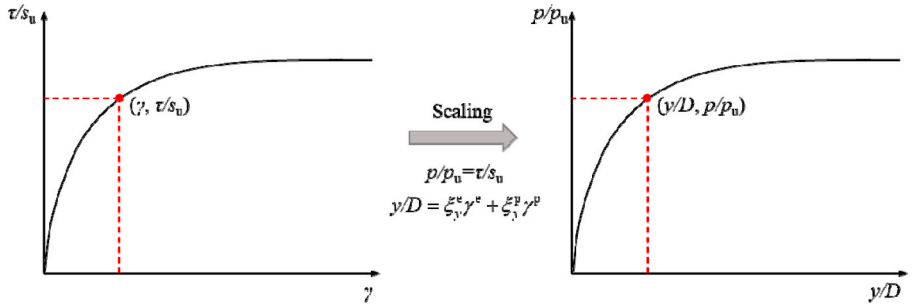 $\frac{p}{p_u}=\frac{\tau}{s_u}$; $\frac{y}{D}=\xi_y^e\gamma^e+\xi_y^p\gamma^p$; $\gamma^e=\frac{\tau}{G_{max}}$; $\gamma^p=\gamma-\gamma^e$ $\xi_y^e=2.8$; $\xi_y^p=1.35+0.25\alpha$ $p_u=N_p s_u D$ $N_p=2[N_1-(N_1-N_2)\frac{z/D}{d})(\frac{z/D}{d})(\frac{z/D}{d})^{0.6})^{1.35}-(1-\alpha)]\le N_{pd}$ $N_{pd}=9.14+2.8\alpha$; $N_1=11.94$; $N_2=3.22$; $d=16.8\text{–}2.3\log_{10}(\lambda)$; $\lambda=s_{um}/kD$; $0.1\le\lambda\le10$ **Site-specific M_R-θ_R curves:** 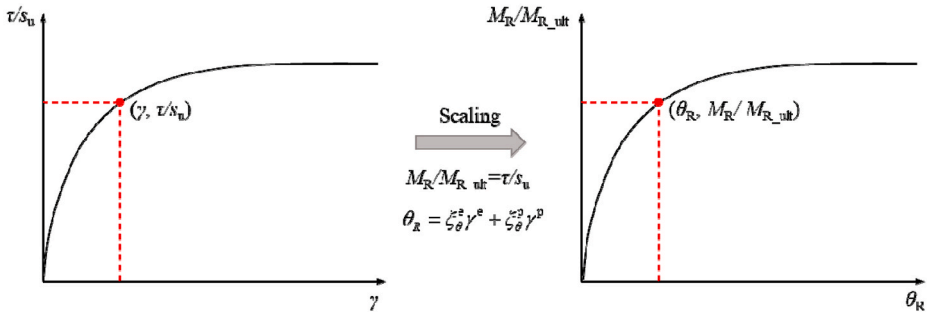 $\frac{M_R}{M_{R\_ult}}=\frac{\tau}{s_u}$; $\theta_R=\xi_\theta^e\gamma^e+\xi_\theta^p\gamma^p$; $\gamma^e=\frac{\tau}{G_{max}}$; $\gamma^p=\gamma-\gamma^e$ $\xi_\theta^e=0.63+0.32(\frac{H}{D})$; $\xi_\theta^p=0.34+0.19(\frac{H}{D})$; $M_{R\_ult}=(\frac{1}{6}\pi D^3 s_{u0}+\pi s_{u0}DH^2)+k(\frac{1}{2}D^2+2H^2)^2[\frac{3}{8}t+\frac{1}{4}\sin(2t)+\frac{1}{32}\sin(4t)]+0.73(\frac{2\pi}{3}s_{u0}H^3+kH^4)$ $t=\arcsin(\frac{D}{\sqrt{D^2+4H^2}})$

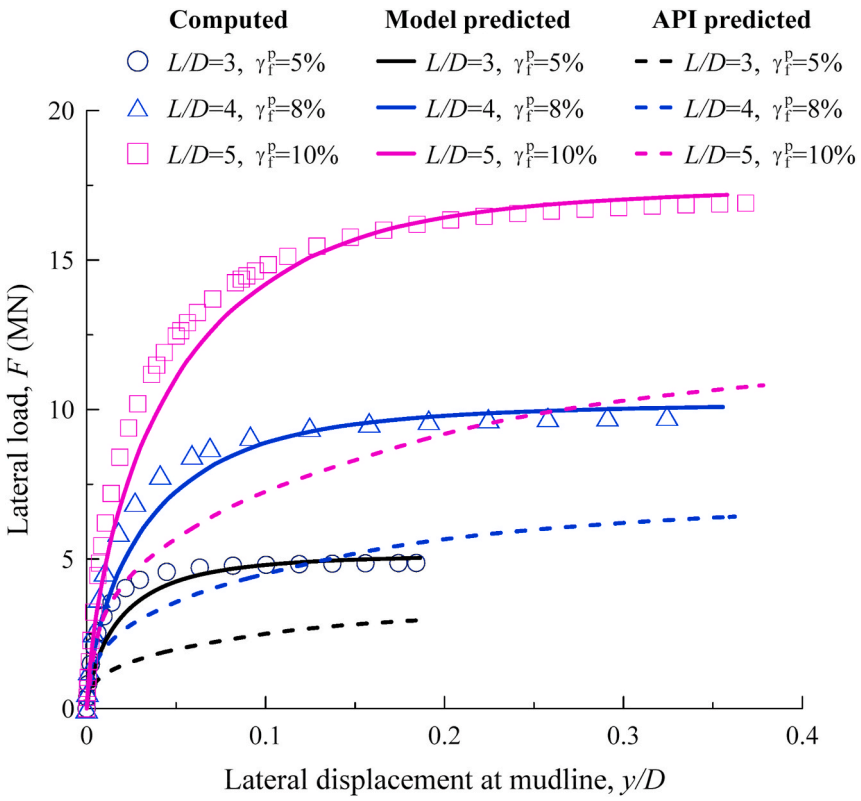

Fig. 13. Validation against finite element analysis on load-displacement relationship.

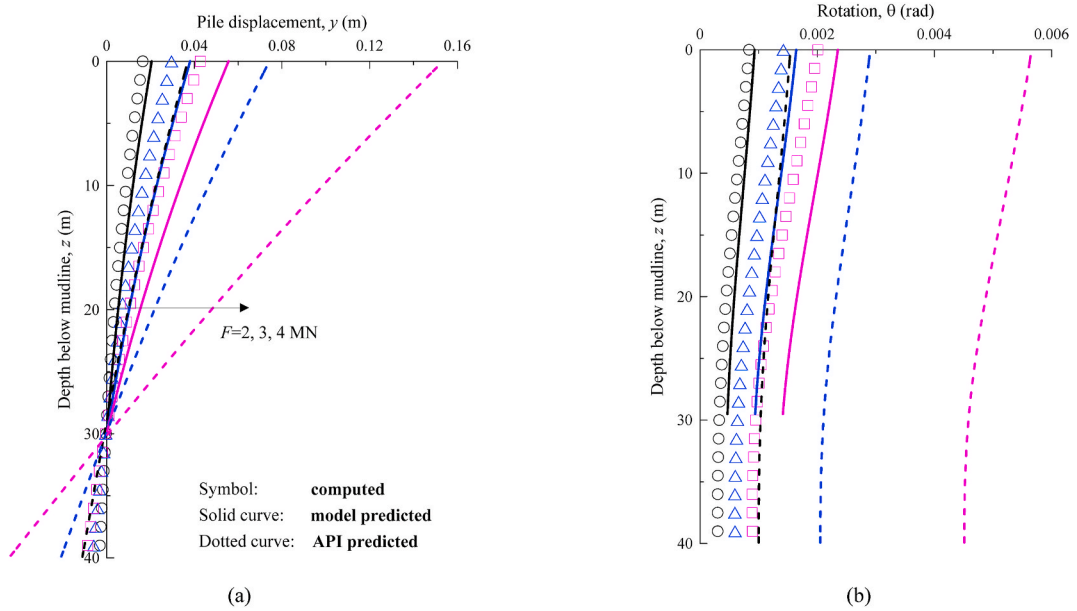

Fig. 14. Validation against finite element analysis on (a) lateral displacement profile and (b) rotation profile of the monopile with $L/D = 5$.

Fig. 15 compares the M_R-θ_R curves at the pile rotation point extracted from the finite element analyses of the full-length pile models and predicted by the proposed model. As illustrated, the model predicted M_R-θ_R curves, which are established by directly scaling the soil stress-strain curve, match well with the computed results, demonstrating the accuracy of the proposed M_R-θ_R model.

6.2. *Validation against centrifuge monopiles tests reported by Murali et al. (2015, 2019)*

Murali et al. (2015, 2019) reported a series of centrifuge tests on a rigid monopile with a prototype diameter of 3.47 m in normally consolidated soft clay. The model pile has a wall thickness of 0.042 m (in prototype) and an embedded length of 7.1 m (in prototype), leading to a L/D ratio of 2. Four load eccentricities, i.e., $e = 1.2$, 1.5, 2.5, and $3.5D$ were examined. The tests with the load eccentricity of 1.2 and $3.5D$ were

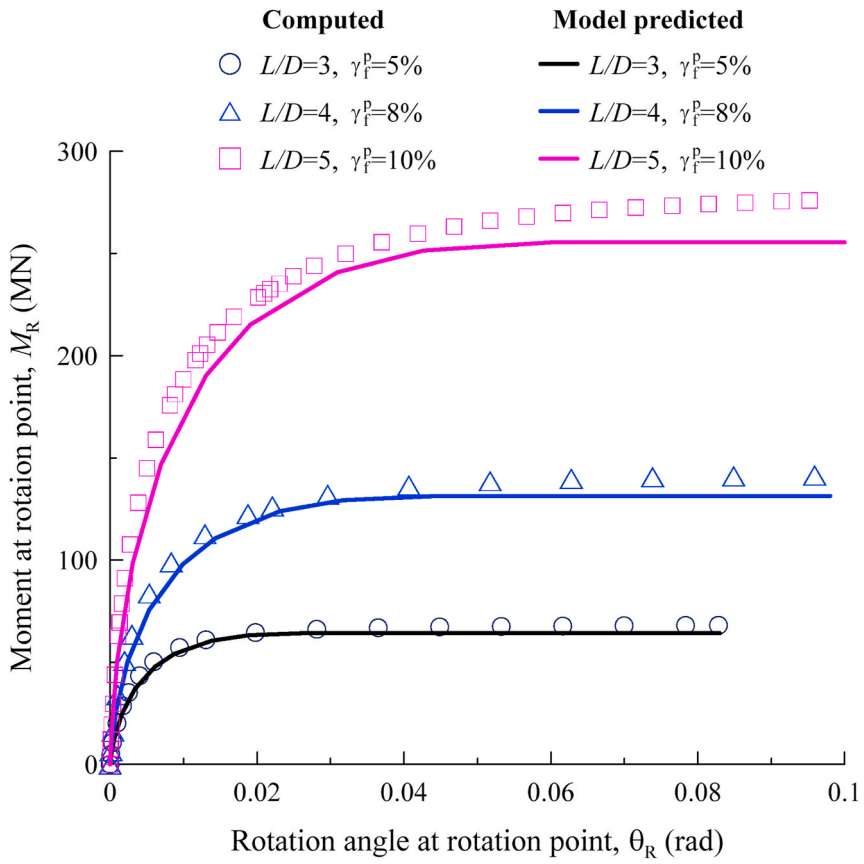

Fig. 15. Validation against finite element analyses of full length monopiles on M_R-θ_R curves.

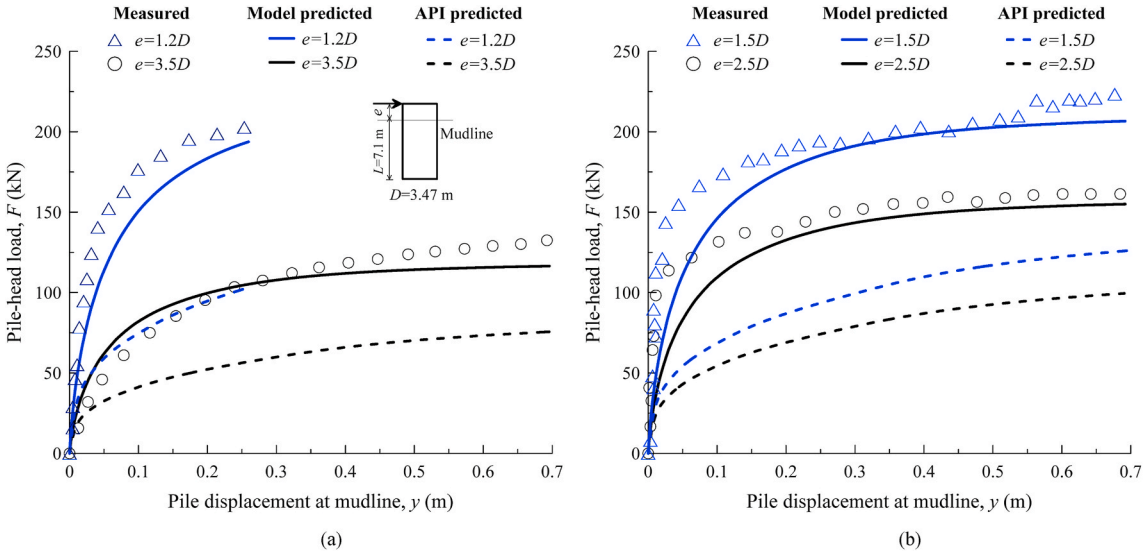

Fig. 16. Validation against centrifuge pile tests performed by Murali et al. (2015, 2019) on load-displacement relationship of the rigid monopile ($D = 3.47$ m, $L/D = 2$) in (a) clay bed 1 and (b) clay bed 2.

carried out in clay bed 1, which has an undrained strength profile of $s_u = 1 + 1.1z$. The tests with the load eccentricity of 1.5 and 2.5D were conducted in clay bed 2 which has an undrained shear strength profile of $s_u = 1 + 1.3z$.

The soil used in their centrifuge tests was the BASF kaolin clay, which has a plasticity index (I_p) of 33%. Due to the lack of reported soil element tests on this kaolin clay, the stress-strain response of the UWA kaolin clay ($G_{max}/s_u = 500$ and $\gamma_f^p = 5\%$) is adopted in the back-analyses (Zhang et al., 2020). The properties of the UWA kaolin are selected because of its comparable plasticity index (28%).

Fig. 16 compares the measured and predicted load-displacement relationship of the monopile at four load eccentricities. The results predicted by the API p-y model are also included in the figure for comparison. As illustrated, the API p-y model grossly underestimates the pile response. On the other hand, the predicted pile response by the proposed model agrees well with those measured from the tests, indicating the

superiority of the proposed model for monopile analysis. For the extremely short monopiles examined ($L/D = 2$) in this validation, the soil resistance from the pile tip is essential. This validation demonstrates that the proposed model can successfully capture the soil resistance below the rotation point.

7. Limitations

In the current study, the soil has been simplified as an isotropic material. However, natural soil exhibits anisotropic strength and stress-strain response. This aspect is to be investigated in further studies. For the monopile foundation under lateral loading, mixed shearing modes are mobilised. For example, the triaxial extension and DSS shearing modes are mobilised by the passive soil wedge while the triaxial compression and DSS shearing modes are mobilised by the active soil wedge. The rotational scoop mobilises the three different shearing modes along different parts of the mechanism. As an interim recommendation, the shear strength and stress-strain response measured in the DSS shear model is suggested to be used when applying the proposed model as the DSS strength is found to be typically a good average of triaxial compression, DSS and triaxial extension strengths (Andersen et al., 2008; Liedtke et al., 2019).

It should be also noted that the proposed site-specific 'p-y + M_R-θ_R' model in this study assumes that the pile section below the rotation point is embedded entirely within a single soil layer with a constant or linearly increasing strength profile. For the case in which the soil below rotation point is layered, engineering judgement is called on to simplify the soil profile into a single layer. However, if the strengths or the stress-strain responses are strongly contrasted between the layers, a site-specific calibration of the M_R-θ_R using the proposed simplified finite element approach might be justified.

8. Summary and conclusions

This paper proposes a site-specific 'p-y + M_R-θ_R' framework for the design of laterally loaded monopiles in soft clay. The lateral soil resistance above the rotation point is represented by distributed p-y springs, while the soil resistance below the rotation point is lumped into a concentrated M_R-θ_R spring. The p-y model proposed by Zhang and Andersen (2017) which scales the p-y curves from the stress-strain response of the soil is adopted to capture the distributed soil resistance above the rotation point. Special attention is paid on the construction of the M_R-θ_R spring from the site-specific stress-strain response and the undrained shear strength profile. Based on the combined analytical analyses and an extensive parametric finite element study, the following conclusions can be drawn:

1. The ultimate moment capacity M_{R_ult} of the M_R-θ_R curves is the sum of the moment resistance due to the scoop failure surface and side shear. A closed-form solution of M_{R_ult} is proposed in this study through an upper-bound analysis, which is a function of pile diameter, the pile length below the rotation point and soil strength profile.
2. The shape of M_R-θ_R curves bear strong similarities to the soil stress-strain curves. A soil with stiffer stress-strain response results in stiffer M_R-θ_R response. When the pile length below the rotation point increases, the M_R-θ_R response becomes gradually softer. While the soil strength heterogeneity exhibits negligible impact on it.
3. The M_R-θ_R response can be well scaled from the stress-strain response of the soil by introducing two scaling factors applied to the elastic and plastic components of the shear stain. These two factors show an approximately linear relationship with H/D.
4. With the proposed site-specific 'p-y + M_R-θ_R' model, soil reaction curves for monopile analysis can be readily constructed based on the stress-strain response of the soil measured in routine soil element tests and shear strength profile established from site characterisation. This provides practising engineers with a simple yet powerful approach to use site-specific soil reaction curves in monopile design.
5. Validations against finite element analyses and centrifuge pile load tests demonstrate the satisfactory predictive capabilities of the proposed model. On the other hand, the conventional API p-y model is proven to significantly underestimate the pile stiffness and capacity. The adoption of the proposed model has large potential for achieving safer and more optimized monopile designs.

CRediT authorship contribution statement

Yongqing Lai: Conceptualization, Methodology, Validation, Investigation, Writing - original draft. **Lizhong Wang:** Conceptualization, Methodology, Writing - review & editing. **Youhu Zhang:** Conceptualization, Methodology, Writing - review & editing. **Yi Hong:** Conceptualization, Methodology, Writing - review & editing.

Declaration of competing interest

The authors declare that they have no known competing financial interests or personal relationships that could have appeared to influence the work reported in this paper.

Acknowledgements

The authors gratefully acknowledge the financial support provided by National Key Research and Development Program of China (2018YFE0109500), National Natural Science Foundation of China (51939010 and 51779221), the Key Research and Development Program of Zhejiang Province (2018C03031) and Joint Fund of Ministry of Education for Pre-research of Equipment (6141A02022137).

References

Achmus, M., Thieken, K., 2016. Evaluation of p-y approaches for large diameter monopiles in soft clay. In: Proceedings of the 26th international ocean and polar engineering conference (isope), pp. 805–816.

Andersen, K.H., Lunne, T., Kvalstad, T.J., Forsberg, C.F., 2008. Deep water geotechnical engineering. In: Proc., XXIV Nat. Conf. Of the Mexican Soc. of Soil Mechanics. Aguascalientes, Mexico, p. 2008.

Abaqus, 2014. Abaqus 6.14 Standard. Dassault Systemes Simulia Corp, Providence, RI, USA.

API Recommended Practice 2GEO, 2014. Geotechnical and Foundation Design Considerations. Addendum 1, Published by the, first ed. American Petroleum Institute. April 2014.

Bransby, M.F., 1999. Selection of p-y curves for the design of single laterally loaded piles. Int. J. Numer. Anal. Methods GeoMech. 23, 1909–1926.

Burd, H., Byrne, B., McAdam, R., Houlsby, G., Martin, C., Beuckelaers, W.J.A.P., Zdravković, L., Taborda, D.M.G., Potts, D.M., Jardine, R.J., Gavin, K., Doherty, P., Igoe, D., Skov, G.J., Pacheco, A.M., Muir, W.A., 2017. Design aspects for monopile foundations. In: Proceeding 19th ICSMGE, Seoul, pp. 35–44.

Byrne, B.W., McAdam, R.A., Burd, H., Houlsby, G.T., Martin, C.M., Beuckelaers, W.J.A.P., Zdravkovic, L., Taborda, D.M.G., Potts, D.M., Jardine, R.J., Ushev, E., Liu, T., Abadias, G.D., Gavin, K., Igoe, D., Doherty, P., Skov, G.J., Pacheco, A.M., Muir, W.A., Schroeder, F.C., Turner, S., Plummer, M.A.L., 2017. PISA: new design methods for offshore wind turbine monopiles. In: Proceedings of the Society for Underwater Technology Offshore Site Investigation and Geotechnics 8th International Conference, London.

Byrne, B.W., McAdam, R.A., Burd, H.J., Beuckelaers, W.J.A.P., Gavin, K., Houlsby, G.T., Igoe, D., Jardine, R.J., Martin, C.M., Muir Wood, A., Potts, D.M., Skov Gretlund, J., Taborda, D.M.G., Zdravković, L., 2019. Monotonic lateral loaded pile testing in a stiff glacial clay till at Cowden. Geotechnique. https://doi.org/10.1680/jgeot.18.pisa.003.

Chortis, G., Askarinejad, A., Prendergast, L.J., Li, Q., Gavin, K., 2020. Influence of scour depth and type on p–y curves for monopiles in sand under monotonic lateral loading in a geotechnical centrifuge. Ocean. Eng. 197, 106838.

Doherty, P., Gavin, K., 2012. Laterally loaded monopile design for offshore wind farms. In: Proceedings of the institution of civil engineers-energy, 165, pp. 7–17, 1.

Fu, D., Zhang, Y., Aamodt, K.K., Yan, Y., 2020a. A multi-spring model for monopile analysis in soft clays. Mar. Struct. 72 (2020), 102768.

Fu, D., Zhang, Y., Yan, Y., Jostad, H.P., 2020b. Effects of tension gap on the holding capacity of suction anchors. Mar. Struct. 69, 102679.

Gao, F.P., Li, J.H., Qi, W.G., Cun, H., 2015. On the instability of offshore foundations: theory and mechanism. Sci. China Phys. Mech. Astron. 58 (12), 124701.

Efthymiou, G., Gazetas, G., 2019. Elastic stiffnesses of a rigid suction caisson and its cylinder sidewall shell. J. Geotech. Geoenviron. Eng. 145 (2), 06018014.

Gerolymos, N., Gazetas, G., 2006. Development of Winkler model for static and dynamic response of caisson foundations with soil and interface nonlinearities. Soil Dynam. Earthq. Eng. 26 (5), 363–376.
Grimstad, G., Andresen, L., Jostad, H.P., 2012. NGI-ADP: anisotropic shear strength model for clay. Int. J. Numer. Anal. Methods GeoMech. 36 (4), 483–497.
He, B., Lai, Y.Q., Wang, L.Z., Hong, Y., Zhu, R.H., 2019. Scour effects on the lateral behavior of a large-diameter monopile in soft clay: role of stress history. J. Mar. Sci. Eng. 7 (170), 1–23.
Hong, Y., He, B., Wang, L.Z., Wang, Z., Ng, C.W.W., Mašín, D., 2017. Cyclic lateral response and failure mechanisms of semi-rigid pile in soft clay: centrifuge tests and numerical modelling. Can. Geotech. J. 54 (6), 86–824.
ISO 19901-4. Petroleum and Natural Gas Industries-specific Requirements for Offshore Structures —Part 4: Geotechnical and Foundation Design Considerations.
Jeanjean, P., 2009. Re-assessment of *p-y* curves for soft clays from centrifuge testing and finite element modeling. In: Proc. Offshore Technology Conf. Paper OTC20158, Houston.
Jeanjean, P., Zhang, Y., Zakeri, A., Andersen, K.H., Gilbert, R., Senanayake, A., 2017. A Framework for Monotonic P-Y Curves in Clays. Keynote Lecture. OSIG SUT conference, London, 2017.
Jostad, H.P., Andersen, K.H., 2015. Calculation of undrained holding capacity of suction anchors in clays. In: Meyer, (Ed.) (Ed.), Offshore Geotechnics III –. Taylor & Francis Group, London.
Kim, Y., Jeong, S., 2011. Analysis of soil resistance on laterally loaded piles based on 3D soil–pile interaction. Comput. Geotech. 38 (2), 248–257.
Klar, A., Osman, A.S., 2008. Load-displacement solutions for piles and shallow foundations based on deformation fields and energy conservation. Geotechnique 58, 581–589.
Lai, Y.Q., Wang, L.Z., Hong, Y., He, B., 2020. Centrifuge modeling of cyclic lateral behavior of large-diameter monopiles in soft clay: effects of episodic cycling and reconsolidation. Ocean. Eng. 200, 107048.
Lam, I.P.O., 2009. Diameter Effects on *P–Y* Curves. Deep Foundations Institute, Hawthorne, N.J.
Liedtke, E., Andersen, K.H., Zhang, Y., Jeanjean, P., 2019. Monotonic and cyclic soil properties of gulf of Mexico clays. In: Offshore Technology Conference (OTC 2019), 6-9 May 2019, Houston, OTC-29622-MS.
Matlock, H, 1970. Correlations for design of laterally loaded piles in clay. Proceedings of the Offshore Technology Conference. Offshore Technology Conference, Houston, TX, USA, pp. 577–588.
Murali, M., Grajales, F., Beemer, R.D., Aubeny, C.P., Biscontin, G., 2019. Capacity of short piles and caissons in soft clay from geotechnical centrifuge tests. J. Geotech. Geoenviron. Eng. 145 (10), 04019079.
Murali, M., Grajales, F., Beemer, R.D., Biscontin, G., Aubeny, C., 2015. Centrifuge and numerical modeling of monopiles for offshore wind towers installed in clay. In: ASME 2015 34th International Conference on Ocean, Offshore and Arctic Engineering. American Society of Mechanical Engineers.
Murphy, G., Igoe, D., Doherty, P., Gavin, K., 2018. 3D FEM approach for laterally loaded monopile design. Comput. Geotech. 100, 76–83.
Osman, A.S., Bolton, M.D., 2005. Simple plasticity-based prediction of the undrained settlement of shallow circular foundations on clay. Geotechnique 55 (6), 435–447.
Osman, A.S., White, D.J., Britto, A.M., Bolton, M.D., 2007. Simple prediction of the undrained displacement of a circular surface foundation on non-linear soil. Geotechnique 57 (9), 729–737.
Qi, W.G., Tian, J.K., Zheng, H.Y., Wang, H.Y., Yang, J., He, G.L., Gao, F.P., 2014. Bearing capacity of the high-rise pile cap foundation for offshore wind turbines. In: International Conference on Sustainable Development of Critical Infrastructure.
Randolph, M.F., Gourvenec, S., 2011. Offshore Geotechnical Engineering. Taylor & Francis.
Wang, L.Z., Lai, Y.Q., Hong, Y., Masin, D., 2020. A unified lateral soil reaction model for monopiles in soft clay considering various length-to-diameter (*L/D*) ratios. Ocean. Eng. 212, 107492.
Wang, X.F., Zeng, X.W., Li, J.L., Yang, X., Wang, H.J., 2018. A review on recent advancements of substructures for offshore wind turbines. Energy Convers. Manag. 158, 103–119.
Yu, J., Huang, M.S., Zhang, C.R., 2015. Three-dimensional upper-bound analysis for ultimate bearing capacity of laterally loaded rigid pile in undrained clay. Can. Geotech. J. 52 (11), 1775–1790.
Yu, J., Huang, M., Li, S., Leung, C.F., 2017. Load-displacement and upper-bound solutions of a loaded laterally pile in clay based on a total-displacement-loading EMSD method. Comput. Geotech. 83, 64–76, 2017.
Zhang, Y., Andersen, K.H., 2019. Soil reaction curves for monopiles in clay. Mar. Struct. 65, 94–113.
Zhang, Y., Andersen, K.H., 2017. Scaling of lateral pile *p-y* response in clay from laboratory stress-strain curves. Mar. Struct. 53, 124–135.
Zhang, Y., Andersen, K.H., Jeanjean, P., 2020. Verification of a framework for cyclic *p-y* curves in clay by hindcast of Sabine River, SOLCYP and centrifuge laterally loaded pile tests. Appl. Ocean Res. 97, 102085.
Zhang, Y., Andersen, K.H., Tedesco, G., 2016. Ultimate bearing capacity of laterally loaded piles in clay-some practical considerations. Mar. Struct. 50, 260–275.
Zhu, B., Zhu, Z.J., Li, T., Liu, J.C., Liu, Y.F., 2017. Field tests of offshore driven piles subjected to lateral monotonic and cyclic loads in soft clay. J. Waterw. Port, Coast. Ocean Eng. 143 (5), 05017003.